

PCCP

Accepted Manuscript



This is an *Accepted Manuscript*, which has been through the Royal Society of Chemistry peer review process and has been accepted for publication.

Accepted Manuscripts are published online shortly after acceptance, before technical editing, formatting and proof reading. Using this free service, authors can make their results available to the community, in citable form, before we publish the edited article. We will replace this *Accepted Manuscript* with the edited and formatted *Advance Article* as soon as it is available.

You can find more information about *Accepted Manuscripts* in the [Information for Authors](#).

Please note that technical editing may introduce minor changes to the text and/or graphics, which may alter content. The journal's standard [Terms & Conditions](#) and the [Ethical guidelines](#) still apply. In no event shall the Royal Society of Chemistry be held responsible for any errors or omissions in this *Accepted Manuscript* or any consequences arising from the use of any information it contains.

Structural differences between the active sites of the Ni-A and Ni-B states of the [NiFe] Hydrogenase: an approach by quantum chemistry and single crystal ENDOR spectroscopy

Jessica L. Barilone, Hideaki Ogata, Wolfgang Lubitz* and Maurice van Gastel*

Max Planck Institute for Chemical Energy Conversion, Stiftstr. 34-36, D-45470 Mülheim an der Ruhr, Germany

Email: wolfgang.lubitz@cec.mpg.de, maurice.van-gastel@cec.mpg.de

Abstract

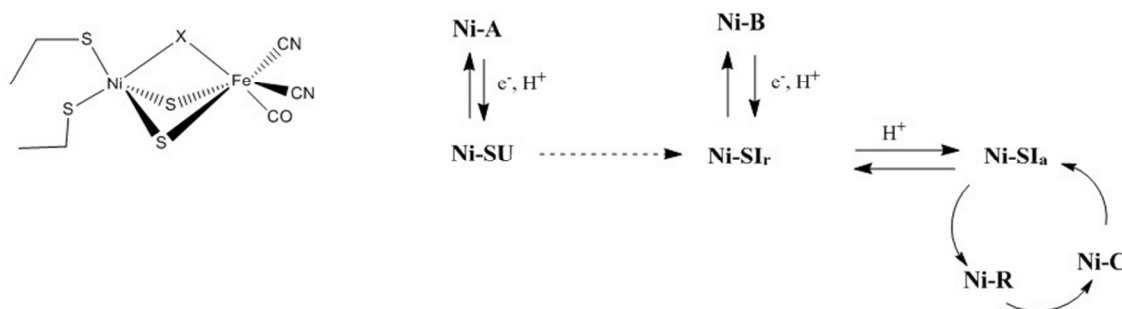
The two resting forms of the active site of [NiFe] hydrogenase, Ni-A and Ni-B, have significantly different activation kinetics, but reveal nearly identical spectroscopic features which suggest the two states exhibit subtle structural differences. Previous studies have indicated that the states differ by the identity of the bridging ligand between Ni and Fe; proposals include OH^- , OOH^- , H_2O , O^{2-} , accompanied by modified cysteine residues. In this study, we use single crystal ENDOR spectroscopy and quantum chemical calculations within the framework of density functional theory (DFT) to calculate vibrational frequencies, ^1H and ^{17}O hyperfine coupling constants and g values with the aim to compare these data to experimental results obtained by crystallography, FTIR and EPR/ENDOR spectroscopy. We find that the Ni-A and Ni-B states are constitutional isomers that differ in their fine structural details. Calculated vibrational frequencies for the cyano and carbonyl ligands and ^1H and ^{17}O hyperfine coupling constants indicate that the bridging ligand in both Ni-A and Ni-B is indeed an OH^- ligand. The difference in the isotropic hyperfine coupling constants of the $\beta\text{-CH}_2$ protons of Cys-549 is sensitive to the orientation of Cys-549; a difference of 0.5 MHz is observed experimentally for Ni-A and 1.9 MHz for Ni-B, which results from a rotation of 7 degrees about the $\text{C}\alpha\text{-C}\beta\text{-S}\gamma\text{-Ni}$ dihedral angle. Likewise, the difference of the intermediate g value is correlated with a rotation of Cys-546 of about 10 degrees.

Introduction

In recent years the pursuit for new, sustainable solutions for energy storage has become a focal point of scientific research and development. A vast area of chemical research is dedicated to developing catalysts that mimic enzymes for small molecule activation.¹ Often, the most efficient mechanisms for catalyzing important chemical reactions such as the reduction of protons to molecular hydrogen, the splitting of water, and the reduction of carbon dioxide can be found in nature. These natural catalysts typically are proteins with metal atoms in their active sites which have evolved over millions of years to efficiently catalyze these otherwise difficult chemical processes.

Hydrogenases comprise an important class of metalloenzymes that are found in a variety of bacteria and archaea, which catalyze the reversible heterolytic oxidation of molecular hydrogen; $\text{H}_2 \rightleftharpoons \text{H}^+ + \text{H}^- \rightleftharpoons 2\text{H}^+ + 2\text{e}^-$. Three classes of hydrogenases are known that are categorized by the metal content of the active site; [Fe], [FeFe], and [NiFe].^{2,3} The class of [NiFe] hydrogenases is the most common class. Heterolytic cleavage of molecular hydrogen is no small feat, since it takes significantly more energy than homolytic cleavage owing to the energy required for separating the charges. Understanding the mechanism behind this important chemical reaction would contribute greatly to the continued pursuit of the use of hydrogen as a clean fuel and the development of efficient biomimetic catalysts.⁴⁻⁶

The [NiFe] hydrogenase has several oxidized forms and two resting states that are referred to as the Ni-A and Ni-B states, in which the valence state of nickel and iron are formally 3+ and 2+, respectively.⁷ The Ni-A state has significantly slower activation kinetics than the Ni-B state.⁸ Upon one electron reduction the Ni-A state converts to the Ni-SU state (EPR silent, unready), while the Ni-B state proceeds to the Ni-SI_r state (EPR silent, ready). Interestingly, the Ni-SU state can convert into the Ni-SI_r state which in turn converts into the active component of the catalytic cycle (Scheme 1).⁹⁻¹² The Ni-A state is of particular interest for investigation due to its low activation kinetics.⁸ Understanding the structural differences between the two resting forms would give valuable insight into the catalytic cycle and the oxygen sensitivity of the enzyme and has been a topic of ongoing investigation. Two major challenges in establishing the structural origin of the different activation kinetics exist. First, the Ni-A and Ni-B states are spectroscopically extremely similar.¹³ Secondly, pioneering work by van Schooneveld and DeBeer has recently shown that the oxidized samples are prone to damage owing to photoreduction inherent to the high intensity of the employed X-ray beam, which may lead to creation of reduced or otherwise damaged species, accompanied by superpositions of structures in the diffraction data.¹⁴



Scheme 1. (Left) Schematic structure of the active site and (right) the catalytic cycle of [NiFe] hydrogenase.¹¹ The dotted arrow connecting Ni-SU to Ni-SI_r represents the slowest step, associated with the largest time constant.^{10, 15} The bridging ligand “X” is a hydroxide for Ni-B¹⁶ and a hydride for Ni-C,¹⁷ for Ni-A its identity is still under debate.

The heterobimetallic active site of [NiFe] hydrogenase has a unique geometry. The nickel and iron atom are bridged by two cysteine residues and one bridging ligand that contains oxygen (in the oxidized state).¹⁸ The iron is additionally coordinated by two cyano groups and one carbonyl group, while the nickel atom is terminally coordinated by two cysteine residues.¹⁹ Previously, crystallographic data suggested that the Fe-coordinated ligands differ between the Ni-A and Ni-B states,¹⁸ however FTIR spectroscopy clearly identifies the ligands to iron as two cyano ligands and one carbonyl ligand.²⁰⁻²² The identity of the bridging ligand in the Ni-B state has been confirmed to be a hydroxide,²³ while it remains under discussion in the Ni-A state. Previous studies have proposed that the bridging ligand in the Ni-A state could be a hydroxide,²⁴⁻²⁷ hydroperoxide,^{18, 28} or oxo ligand.²⁹ Many theoretical studies have been conducted in an effort to elucidate the structural differences between the Ni-A and Ni-B states.^{9, 24, 27, 29-38} Most notably Li and Hall in 2001 performed calculations on multiple model structures for the Ni-A state and found that a hydroxide bridge is most likely, albeit with a reduced, protonated thiolate.²⁴ Recent work by Pardo et al²⁷ predicted a sulfenated cysteine as well as a hydroperoxo bridging ligand, following previous suggestions by Volbeda et al.²⁸ The latest crystal structure determination by Volbeda et al,³⁹ however, contains an oxygenated thiolate, S=O and a hydroxide bridge. A misconception is that O₂ is required for formation of Ni-A; Albracht et al have shown that oxidation with molecular oxygen exclusively gives rise to the Ni-B state within 158 ms.²² Additionally, O₂ is a triplet state, and the presence of an intact O₂ molecule near the active site would completely alter the EPR spectrum. It is thus clear that agreement amongst the scientific community as to the composition of the Ni-A state has so far still not been achieved.

The three most accessible spectroscopic parameters that can be used to investigate the active sites of the Ni-A and Ni-B states are the vibrational frequencies (by FITR spectroscopy),⁴⁰ the g-tensor (by EPR spectroscopy),⁷ and the isotropic hyperfine coupling constants (by ENDOR spectroscopy).²³ Alone, neither of them provides conclusive hints as to the structural differences of Ni-A and Ni-B. However, taken together and complemented with quantum chemical calculations, these spectroscopic parameters can be used to critically verify whether or not structural models for the Ni-A state, mainly from X-ray crystallography, are in agreement with

the spectroscopy.

The goal of this study is to investigate the structural differences between the Ni-B and Ni-A oxidation states of [NiFe] hydrogenases. We employ quantum chemical calculations and single-crystal ENDOR spectroscopy to achieve this goal. The latter spectroscopy is used in order to obtain a complete data set of experimental hyperfine coupling constants of protons at the active site. The initial structures of the models for the active site used in the calculations are based on recent and older structural proposals based on experiments using X-ray crystallography.

Methodology

All calculations were performed using the ORCA quantum chemistry software package (Version 3.1).⁴¹ Frequency calculations for all models were carried out following the geometry optimizations using the BP86^{42, 43} functional in conjunction with the RI-J approximation and dispersion correction (D3BJ).^{44, 45} Single point EPR calculations were performed with the B3LYP functional⁴⁶ and the RI-JCOSX⁴⁷ approximation.

Small Models

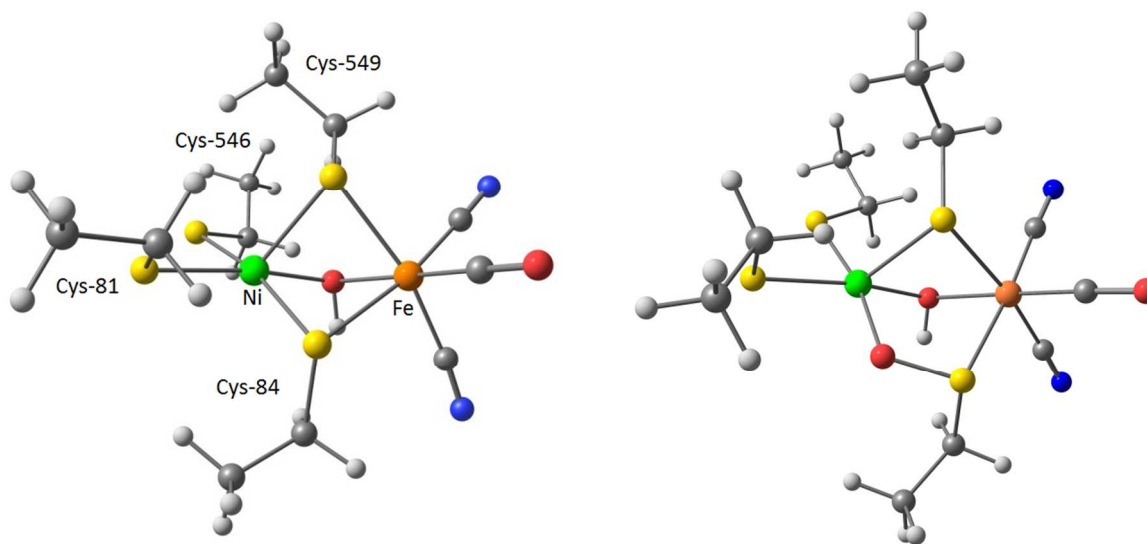


Figure 1. (left) Small OH α model; (right) first coordination sphere of the S=O OH α model used for the structure by Volbeda et al.³⁹ Color coding: hydrogen – white; carbon – grey; oxygen – red; sulfur – yellow; iron – orange; nickel – green.

Small models have been constructed based on the crystal structure of *D. vulgaris* Miyazaki F hydrogenase.¹⁸ Based on the identity of the bridging ligand, the models are named OH α , OH β (hydroxide bridge in two possible conformations), H₂O (bridging water), O²⁻ (bridging oxo) and S=O OH α after the latest structure by Volbeda et al.³⁹ The representative small OH α model is shown schematically in Figure 1. The cartesian coordinates are provided as supporting information.

The zeroth order relative approximation (ZORA) was included in all calculations.^{48, 49} Solvent effects were not taken into account for the small models. Geometry optimization and frequency calculations were performed using the Def2-TZVP^{50, 51} basis set for the Ni, Fe and S atoms, and the Def2-SVP basis set⁵¹ for all other atoms.

Large models

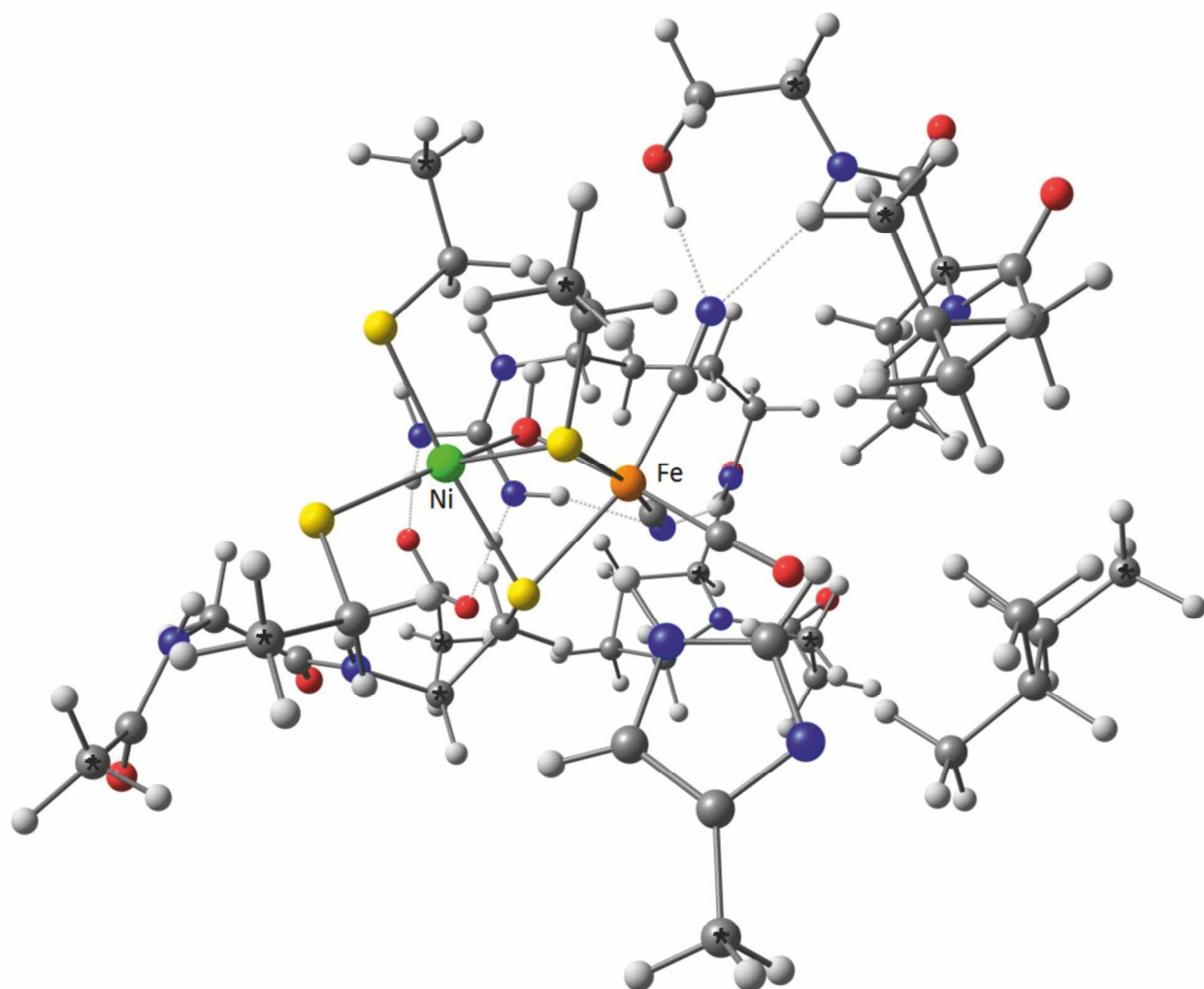


Figure 2. Large OH α model for the active site. Thirteen carbon atoms (*) have been constrained during geometry optimization.

Large models of the active site were used that include the second and third coordination sphere of the protein using a procedure described earlier.¹¹ These models include nearby side chains that stabilize the active site, in particular the hydrogen bonding network to the diatomic ligands at iron. Geometry optimization and vibrational analysis were performed using the zero-order-relative approximation with the Def2-TZVP basis set⁵¹ for the Ni, Fe, S, the CN and CO ligands,

as well as the bridging ligand. The Def2-SVP basis set⁵¹ was used for all other atoms. For the single-point EPR calculations, the basis sets of Ni, Fe and S were enlarged to Def2-TZVPP.⁵¹ Geometry constraints were imposed on 13 carbon atoms in the outer sphere of the models to inhibit the movements and rotations of complete side chains in order to reflect a more realistic protein environment (Figure 2). As a result of the geometry constraints on the system, imaginary vibrational frequencies resulting from the Hessian not being completely positive-definite were observed in all calculations. The largest imaginary frequency occurred at -55 cm^{-1} indicating that the geometry constraints impose only very minor strain on the active site. All calculations on the large models were performed with COSMO (conductor-like screening model)⁵² to include solvation effects on the system by surrounding the system with a dielectric constant, ϵ , of 4.0.^{53,54} The ligand fields at nickel and iron are square pyramidal and octahedral.

Single crystal ENDOR experiments of Ni-A

Single crystal ENDOR experiments have been performed and analyzed as described previously.²³ The hydrogenase was purified and the Ni-A state was prepared by the same methods as used in crystallographic studies in 2005, by addition of Na_2S .¹⁸

Results and Discussion

The Ni-A and Ni-B states are spectroscopically very similar. Besides the different activation kinetics (the activation time constant amounts to several tens of seconds for Ni-B and longer than 10 minutes for Ni-A)¹⁵ and different g_y values, 2.24 for Ni-A and 2.16 for Ni-B, all other spectroscopic characteristics are nearly identical. This strongly indicates that the structural differences between Ni-A and Ni-B near the active site, wherein most spectroscopies are sensitive, must be very small. Therefore, the results section is divided in such a way that spectroscopies that give the same fingerprint for Ni-A and Ni-B are only briefly considered, whereas those that lead to significant and interpretable differences between Ni-A and Ni-B are more elaborately analyzed.

Vibrational Spectroscopy and comparison with crystal structures

The [NiFe] hydrogenase from *D. vulgaris* Miyazaki F has been extensively studied by FTIR spectroscopy.^{13,40,55-58} Interestingly, within the family of [NiFe] hydrogenases, the characteristic CO and CN^- stretching bands differ by $5\text{-}10\text{ cm}^{-1}$ wavenumbers. These differences have not been carefully examined in detail yet, but are presumably the result of small changes in the primary structure of the proteins which modulate the tertiary structure and the strength of the hydrogen bonds to the CN^- ligands. Additionally, the stretching frequencies for the Ni-A and Ni-B states are essentially identical, pointing to very similar if not identical structural compositions of the active site near the Fe. Initial reports by Hall et al provided insight into the structure of the active site in most oxidation states.^{27,34} The Ni-A and Ni-B states were tentatively assigned as a Ni(III)-Fe(II) μ -oxo and Ni(III)-Fe(II) μ -hydroxo species.³⁴ The employed models at that time, however, did not include elements of the hydrogen bonding network around the cyanide ligands, so

accurate calculations of the stretching frequencies of the CO and CN^- ligands remained a challenge. Subsequent experiments, in particular by X-ray crystallography, brought up the discussion again of the Ni-A state with varying reports of a μ -hydroperoxo species²⁸ or μ -hydroxo species^{24, 25} and moreover one, and in some experiments even two additional oxygen atoms attached to the cysteine residues.²⁸ The most recent crystal structure suggests that such an S=O fragment bridges the nickel and iron atom such that a bimetallic cyclopentanyl ring structure ($\sim\text{S-O-Ni-S-Fe}\sim$) exists.³⁹ With such a wide variety of differing proposed crystal structures, we were compelled to systematically reinvestigate the structural propositions, by additionally including as much experimental information as possible from spectroscopy. This concerns for example the stretching frequencies of the CN^- and CO bands in the FTIR spectrum.^{13, 40, 59} The underlying idea is simply that a structural model verified by multiple methods is more reliable than a model proposed by only one method.

Initial small model geometries have been employed that are comprised of cysteine residues modeled as ethylthiolates, a bridging ligand of varying identity, the CO and two CN^- ligands coordinated to iron and nickel. In one additional calculation, the bridging Cys-84 has been changed to include an S=O group with S bound to Fe and O bound to Ni, according to the latest crystal structure. The calculated as well as the experimentally observed frequencies for Ni-A and Ni-B for *D. vulgaris* Miyazaki F hydrogenase are included in Table 1. As becomes clear from the table, none of the calculated frequencies correspond well to the experimentally observed frequencies. This is to be expected especially for the two CN^- stretching frequencies, as the hydrogen bonding network present in the protein is not included in the small models. Still, a number of interesting observations can be made; 1) The di-anionic oxo bridging ligand gives rise to significantly different stretching frequencies than the mono-anionic ligands. 2) The geometry optimization of the molecule with the hydroperoxo bridge, previously thought to be a prime candidate for Ni-A,²⁸ while at the same time based on its very unusual ligand field at nickel deemed unlikely by one of the present authors,²⁵ indeed leads to a complete reorientation of the OOH^- moiety to such large extent that the position of the distal oxygen atom becomes incompatible with the crystal structure where the hydroperoxo ligand was proposed. 3) Geometry optimization of the structure with the neutral H_2O ligand leads to dissociation of water from the iron atom. The trend for the CO stretching frequencies is that the neutral H_2O gives rise to the largest CO frequency (1961 cm^{-1}), the monoanionic bridging ligands to intermediate values ($1904\text{-}1911\text{ cm}^{-1}$), and the di-anionic oxo to the lowest CO frequency of (1836 cm^{-1}), indicating that the CO stretching frequency is sensitive to the charge at iron. 4) Geometry optimization of the latest crystal structure featuring the bimetallic cyclopentane ring gives rise to much smaller deviations from the crystal structure than for the proposed hydroperoxo structure. The inclusion of Cys-84 with an S=O fragment according to the latest structural proposal by Volbeda et al³⁹, as represented by the S=O, $\text{OH}\alpha$ model, apparently does not affect the stretching frequencies as compared to the models $\text{OH}\alpha$ and $\text{OH}\beta$.

Table 1. Experimental and calculated CO and CN stretching frequencies [cm^{-1}] for small and large Ni-A models containing different bridging ligands.

	CO	CN _{antisym}	CN _{sym}
Experimental			
Ni-A ^a	1956	2085	2094
Ni-B ^a	1954	2081	2090
Ni-A ^b	1947	2085	2095
Ni-B ^b	1946	2080	2090
Calculated			
<i>Small Models</i>			
OH α	1905	2073	2088
OH β	1904	2074	2087
H ₂ O	1961	2079	2089
O ²⁻	1836	2044	2058
OOH ⁻	1911	2084	2094
S=O, OH α ^c	1907	2079	2096
<i>Large Models</i>			
OH α	1924	2060	2081
OH β	1924	2056	2086
H ₂ O	1968	2065	2088
O ²⁻	1896	2024	2053
OOH ⁻	1929	2055	2095
S=O, OH α ^c	1928	2068	2093

^a Experimental data for *D. vulgaris* Miyazaki F¹³

^b Experimental data for *D. desulfuricans* hydrogenase.³⁹

^c Model based on the latest crystal structure.³⁹

With this insight, we proceed to examine the larger models that include the hydrogen bonding network. Upon comparing tables 1 and 2, it becomes clear that the frequencies have systematically become lower by approximately 25 cm^{-1} . Based on the calculated CO stretching frequency, and taken into account that calculated metal-carbonyl stretching frequencies systematically underestimate the experimental frequency by approximately 28 cm^{-1} ,^{60,61} the only feasible models are those with a mono-anionic bridging ligand. Thus, the three models that are comparable to experimental data are those with an OH⁻ or OOH⁻ ligand and the model based on the Volbeda structure (S=O, OH α).³⁹ The models with the aquo or oxo bridge do not give rise to stretching frequencies compatible with experiment.

Concerning bond distances, in the latest crystal structure by Volbeda et al, the NiFe distance is reported to be 3.09 \AA and the oxygen of the S=O fragment of Cys-84 coordinates to nickel and the sulfur to iron, thus giving rise to an S₃O₂ first coordination sphere of nickel. Calculations using constrained geometry optimization with the crystal structure as a starting structure increase this distance to 3.13 \AA . This contrasts considerably with earlier structure determinations of Ni-A without a μ -per(sulf)oxo bridging motif of Cys-84 in which the distance was typically 2.80 \AA .¹⁸

Constrained geometry optimization of both structures OH α and OH β indeed give a NiFe distance of 2.83 Å. Unfortunately, EXAFS data are at present not conclusive on the atomistic composition of the direct coordination, as well as on the Ni-Fe distance; the only work reported is by Bagyinka et al. who deduced that the nickel center may be coordinated by 3(\pm 1) oxygen or nitrogen atoms and 2(\pm 1) sulfur atom, seemingly in disagreement with many proposed models.⁶² They also observed a negligible shift of the Ni K-edge upon reduction, thus concluding that no redox activity of the nickel atom could be discerned from the EXAFS data.⁶²

Other modified model geometries have been considered in addition to those reported in Table 1, e.g., one with a neutral arginine, one with a terminal instead of a bridging OH $^-$ ligand or even one with a protonated cysteine. All these rather unlikely models indeed give rise to large changes in the geometry optimization and/or CO and CN $^-$ vibrational frequencies up to 50 cm $^{-1}$ away from the experimental values. In summary, the combined analysis of the calculated and experimental FTIR spectra, as well as critical comparison with the available crystal structures and EXAFS data, in particular with respect to the NiFe distance and the first coordination sphere of nickel, an S $_4$ O coordination as in models OH α and OH β seems to provide best agreement with experimental data. Therefore, these model structures, as well as the latest structure by Volbeda et al.,³⁹ although the latter seems to be not compatible with EXAFS data, will be considered in the following sections.

Hyperfine coupling constants of Ni-A and Ni-B

Table 2. Calculated and experimental ^1H isotropic hyperfine coupling constants [MHz] of the β protons of Cys 549 and bridging hydroxide.

	OH $^-$	Cys-549 H β 1	Cys-549 H β 2	H β 1-H β 2
Experimental				
Ni-A ^a	2.6	11.0	11.5	0.5
Ni-B ^b	-3.9	13.1	11.2	1.9
Calculated				
OH α	-1.6	9.9	12.4	2.5
OH β	1.1	10.0	12.3	2.3
S=O, OH α	0.7	8.2	11.6	3.4
H $_2$ O		2.9	-4.4	7.3
O $^{2-}$		6.3	12.3	6.0

^a Experimental data from this work

^b Experimental data from reference ¹⁶

Additional experimental information is available for the Ni-A and Ni-B states from ENDOR spectroscopy. With ENDOR spectroscopy, in particular on paramagnetic centers in single crystal, sensitive information can be obtained about the spin density distribution. Single crystal ENDOR spectroscopy for the Ni-B state for example allowed for the determination of the full hyperfine tensor of the β -CH $_2$ protons of Cys-549 as well as that for the proton of the bridging OH $^-$ ligand

(isotropic coupling constants are included in table 2).²³ For Ni-A, ^{17}O ENDOR spectroscopy has unequivocally proven the presence of an oxygen-based bridging ligand.⁶³ From these isotope-exchange experiments, it became clear that the bridging ligand is not in contact with the solvent, and isotope exchange only occurred upon reduction and re-oxidation.⁶³ A full ^1H single crystal ENDOR study on a Ni-A crystal in H_2O and one which has been reduced and re-oxidized to Ni-A in D_2O prior to crystallization has been performed and is reported upon in this work. Indeed single crystal ENDOR spectra reveal the presence of an exchangeable proton (Figure 3, top), but with a different isotropic hyperfine coupling constant. The full field-frequency plots are shown in Figure 3. Analysis of the data reveals three hyperfine coupling constants. Hyperfine tensors A1 and A2 (Figure 3, middle and bottom) could be determined fully and belong to the $\beta\text{-CH}_2$ protons of Cys-549. The hyperfine tensor A3 of the exchangeable (i.e. upon reduction and re-oxidation, dashed line in Figure 3(top)) proton could unfortunately not be fully determined owing to the fact that the anisotropy of this signal causes it to overlap with those of weakly coupled protons over a wide range of angles. Nevertheless, analysis reveals that the isotropic coupling constant has to be positive (included in Table 2) and it is furthermore clear that the proton A3 displays a different angular dependence than that observed for the proton of the OH^- bridge in a single crystal ENDOR study of the Ni-B state.^{13,23} For the $\beta\text{-CH}_2$ protons of Cys-549 in the Ni-A state, the full tensors are given in Table 3.

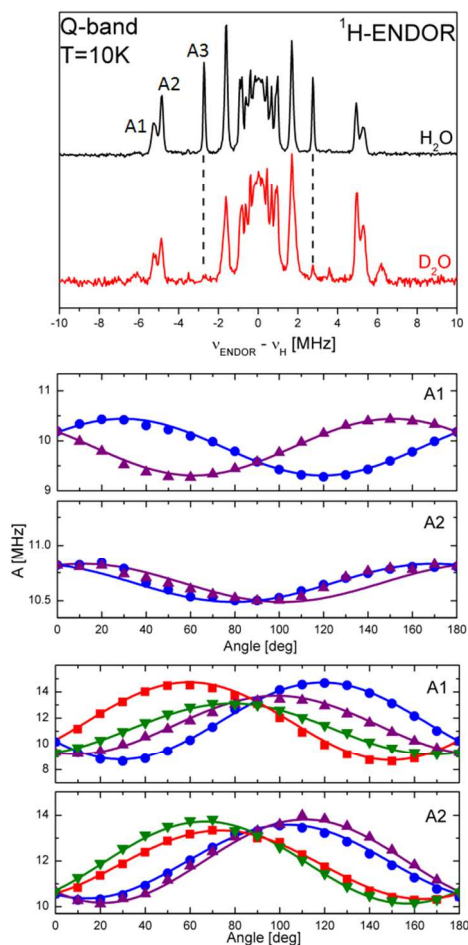


Figure 3. (Top) Single crystal ENDOR spectra of *D. vulgaris* Miyazaki F hydrogenase in the Ni-A state in H₂O and in D₂O after one reduction-reoxidation cycle, reproduced from reference ¹³. (Middle) Orientation dependence with the long axis of the crystal in a vertical position of the two pronounced hyperfine signals A1 and A2 that correspond to the β -CH₂ protons of Cys-549 (A1, A2). (Bottom) Ibid. with the long axis of the crystal in a horizontal position.

Table 3. Experimental hyperfine coupling constants [MHz] and direction cosines of the signals A1 and A2 with respect to the crystallographic-axes (a , b , c) as observed in the ENDOR spectra of *D. vulgaris* Miyazaki F hydrogenase in the Ni-A state.

Principal values				Direction cosines		
				l_{ai}	l_{bi}	l_{ci}
A1		a_{iso}	11.0			
A_x	8.6	A'_x	-2.4	-0.164	0.881	0.444
A_y	14.7	A'_y	3.7	0.324	-0.378	0.868
A_z	7.9	A'_z	-1.3	0.932	0.286	-0.223
A2		a_{iso}	11.5			
A_x	10.0	A'_x	-1.5	-0.113	0.919	0.378
A_y	13.8	A'_y	2.3	-0.131	0.364	-0.922
A_z	10.8	A'_z	-0.7	-0.985	-0.153	0.079

With accurate hyperfine couplings A1 and A2 available for both Ni-A and Ni-B, we now venture to investigate these numbers. In particular, the difference of the isotropic hyperfine coupling constants of the two β -CH₂ protons of Cys-549 amounts to 1.9 MHz for the Ni-B state and 0.5 MHz for the Ni-A state, possibly pointing to a reorientation of the Cys-549 fragment. Therefore, a series of calculations was performed, in which Cys-549 was manually rotated by changing the C α -C β -S γ -Ni dihedral angle. The results are shown in Figure 4. From the figure, it becomes clear that the difference in the isotropic hyperfine coupling constants of H β 1 and H β 2 is a sensitive parameter for the orientation of Cys-549. A difference of 0.5 MHz as observed experimentally for Ni-A is easily obtained by rotation of the dihedral angle by -4 degrees. Similarly, a difference of 1.9 MHz as observed for Ni-B (cf. Table 2) is obtained at a dihedral angle of $+3$ degrees, thus indicating that Cys-549 is oriented differently in Ni-A and Ni-B with respect to the C α -C β -S γ -Ni dihedral angle by about 7 degrees. The rotation is essentially barrierless over a range of ± 10 degrees and the electronic energies differ by maximal 0.07 kcal/mol.

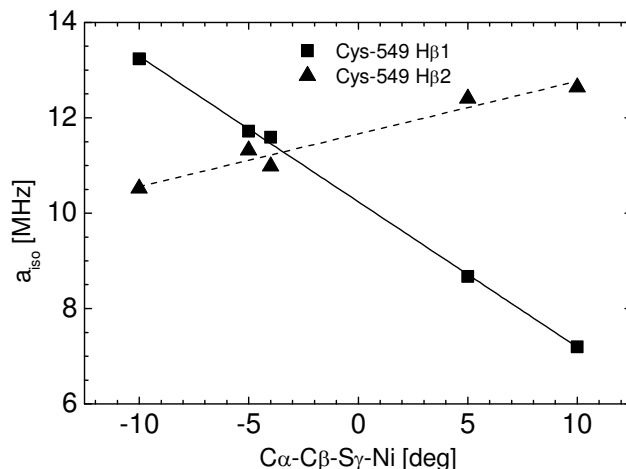


Figure 4. Linear correlation of ^1H isotropic hyperfine coupling constants obtained by manually changing the Cys-549 $\text{C}\alpha\text{-C}\beta\text{-S}\gamma\text{-Ni}$ dihedral angle in the $\text{OH}\alpha$ model. An angle of zero corresponds to the equilibrium position of the fragment in the constrained geometry optimization.

Additional experimental information is available from the ^{17}O hyperfine tensors. Experimentally, ^{17}O ENDOR signals have been measured by Carepo *et al* for the Ni-A state of *D. gigas* hydrogenase and amount to [5, 9, 20] MHz, leading to an isotropic coupling of 11 MHz.⁶³ Moreover, orientation-selected ^{17}O ENDOR spectra presented by Carepo *et al* indicate that the smallest of these components (5 MHz) is attained at an effective g value in between the largest g value ($g_x = 2.32$) and the intermediate g value ($g_y = 2.24$).⁶³ Calculated hyperfine coupling constants (spin contamination is negligible as seen from the computed expectation value of S^2 of 0.78) are included in Table 4. Note that ^{17}O has a negative nuclear g value and that the absolute sign in the experiment cannot be determined. Upon comparison of the absolute values of the numbers in Table 4, it immediately becomes clear that both nickel-coordinated ^{17}O atoms in the new Volbeda structure give rise to coupling constants that mismatch the experiment by up to a factor of 3. In particular, the isotropic ^{17}O hyperfine coupling constants are calculated to be too large. For the $\text{OH}\alpha$ and $\text{OH}\beta$ structures, experiment and theory are in better agreement.

Table 4. Experimental and calculated ^{17}O hyperfine coupling constants [MHz] of the bridging ligand and of the oxygenated Cysteine in the crystal structure ($\text{S}=\text{O}$, $\text{OH}\alpha$) by Volbeda *et al.*³⁹

	A_x	A_y	A_z
Experimental			
Ni-A ^a	5	9	20
Calculated			
$^{17}\text{OH}\alpha$	-2	-4	-13
$^{17}\text{OH}\beta$	-6	-8	-15
$\text{S}=\text{O}$, $^{17}\text{OH}\alpha$ ³⁹	-18	-19	-30
$\text{S}=\text{O}$, $\text{OH}\alpha$ ³⁹	-11	-12	-17

^a Experimental data from reference ⁶³.

g values

The most notable spectroscopic difference between the Ni-A and the Ni-B states is found in their *g* values; this particularly concerns the intermediate *g* value (g_γ) that typically amounts to 2.24 for Ni-A and 2.16 for Ni-B. Of particular difficulty for the interpretation of this difference is the fact that the most commonly used DFT method⁶⁴ has limited accuracy and systematically underestimates the largest *g* shift by up to 30%. Of greater concern is that this method is also known to occasionally give rise to even larger differences of more than 100%, for example for the small molecule TiF₃.⁶⁴ The main inaccuracy of the method has been traced to the overestimation of excitation energies, which is a well-known deficiency of the TD-DFT method as well.⁶⁵ The overestimation of excitation energies leads to an underestimation of the calculated *g* values that, according to equation 1, are a second order property, for which knowledge of the ground state wave function, the excited state wave function and the excitation energies are in principle needed for computation.

$$g_e \begin{pmatrix} 1 & 0 & 0 \\ 0 & 1 & 0 \\ 0 & 0 & 1 \end{pmatrix} + 2 \sum_{k \neq 0} \sum_{A=1}^M \frac{\langle \psi_k | \mathbf{L}_A | \psi_0 \rangle \langle \psi_0 | \xi_A \mathbf{L}_A | \psi_k \rangle}{E_0 - E_k} \quad (1)$$

In this already largely simplified equation, ψ_0 represents the singly occupied molecular orbital of the ground state in a single-reference formalism and the index *k* runs over electronic excited states. The index *A* runs over all nuclei, E_0 and E_k are state energies of the ground state and the *k*-th excited state. The parameter ξ_A is the 1-electron spin-orbit-coupling constant of the *A*-th nucleus and \mathbf{L}_A is the one-electron orbital angular momentum operator for the *A*-th nucleus.⁶⁶

Thus we initially undertake an exploratory investigation that focuses on the possible differences between Ni-A and Ni-B that are relevant for the intermediate *g* value: first, we focus on the singly-occupied molecular orbital of the ground state, ψ_0 . This orbital has been investigated by making use of ENDOR spectroscopy. Interestingly, the ENDOR spectra of the Ni-A and Ni-B states are extremely similar. This is particularly valid for the hyperfine coupling constants of the β -CH₂ of Cys-549 protons. Their difference has been rationalized by a small change of 7 degrees of the C α -C β -S γ -Ni dihedral angle of this cysteine residue in the previous section. The nearly identical ENDOR spectra moreover indicate that the bulk spin density at nickel and S γ (Cys-549), are the same for Ni-A and Ni-B. The singly occupied natural orbital, ψ_0 , of the OH α model is given pictorially in Figure 5. The orbital composition is such that 80% of the spin is located at nickel and 24% at S γ (Cys-549). Thus, for ψ_0 , these atoms account for essentially all spin population, where the other atoms carry very small amounts of negative spin population such that the total spin population equals 100% (See Table S2). In turn, according to equation 1, these are the only two atoms whose spin population may contribute to the *g* values.

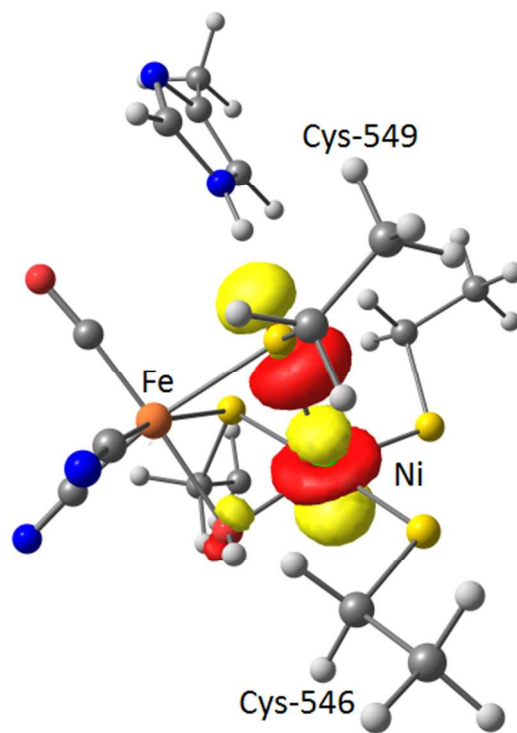


Figure 5. Singly occupied natural orbital ψ_0 for the OH α model. The composition is as following: the d_{z^2} at nickel and $3p_z$ orbital at S γ (Cys-549) contains to 80% and 24% of the spin, respectively. The σ^* interaction between the d_{z^2} orbital at nickel and the $3p_z$ orbital at S γ (Cys-549) is clearly visible. The second coordination sphere has been omitted for clarity.

Next, we focus on the excited states. According to equation 1, the first excited state relevant for the intermediate g value, g_y , would be the one where the singly occupied orbital would have d_{xz} character. This orbital, which is doubly occupied in the ground state, is shown in Figure 6. Particularly striking about this orbital is the observation that the d_{xz} orbital is involved in a covalent π^* interaction with the $3p_z$ orbital of S γ (Cys-546), which carries the largest spin population. A second excited state involving a complementary bonding orbital to the one shown in figure 6 is also relevant. This gives rise to the idea that it may be conceivable that a small angular rotation near Cys-546, similar to the one at Cys-549, may destabilize the d_{xz} orbital and significantly affect the covalency of this π^* interaction, and conversely the π interaction in the lower-lying bonding orbital with dxz character. If the dxz orbital is destabilized, the π^* orbital in Figure 6 would obtain more dxz character, whereas the complementary and lower-lying π would get more sulfur character. This in turn may shift the density related to the d_{xz} orbital from a lower-lying to a higher-lying molecular orbital, and according to equation 1, this would increase the g_y value. We note that a change in the bonding and anti-bonding orbitals with d_{xz} character would not affect the ENDOR spectrum, since the ENDOR spectrum is determined by hyperfine interactions, which are first order properties that depend only on ψ_0 (cf. Figure 5)! As such, a rotation near Cys-546 would be completely in line with experimental data. Thus, the idea comes

up that the different g_y values of Ni-A and Ni-B may not be related to differences in the SOMO, ψ_0 , at all, but rather to differences in the orbitals with d_{xz} character. The invariance of ψ_0 would then explain why the ENDOR spectra of Ni-A and Ni-B are essentially identical as demonstrated by our ENDOR data (*vide infra*), while the g values are not.

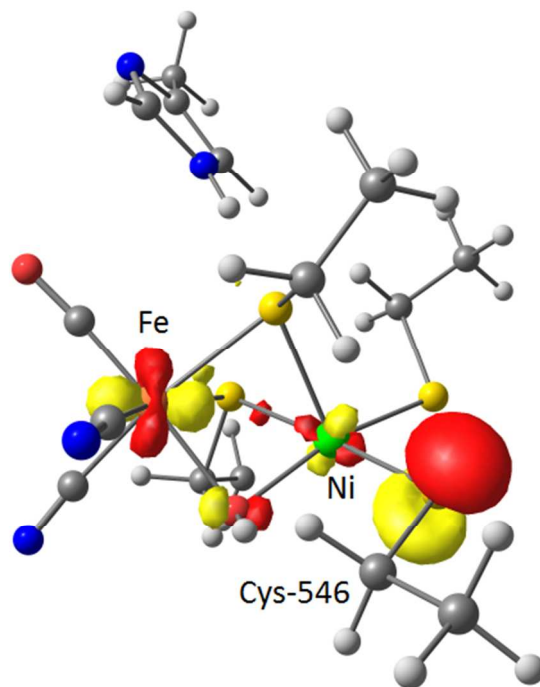


Figure 6. Doubly occupied molecular orbital with d_{xz} character, for the OH α model. This orbital is singly occupied in the excited state relevant for g_y . This orbital is π anti-bonding between the d_{xz} orbital at nickel and a $3p_z$ orbital at $S\gamma$ (Cys-546), which dominates and is located in the front of the figure.

In order to test this hypothesis, the Cys-546 fragment was manually rotated by 10 degrees by changing the $C\alpha$ - $C\beta$ - $S\gamma$ -Ni dihedral angle and an additional calculation has been performed. Of particular notice for this modified geometry is that the plane spanned by nickel, $S\gamma$ (Cys-546) and $C\beta$ (Cys-546) is no longer perpendicular to the molecular z axis (given by the direction from nickel to $S\gamma$ (Cys-549)), and therefore, the Cys-546 residue is less prone to π interactions with nickel. This indeed led to a significant shift of electron density of up to 7% from $S\gamma$ (Cys-546) towards nickel, which in turn would lead to a significantly increased g_y value according to equation 1.

Regrettably but not unexpectedly, the DFT formalism does indeed underestimate both the g_x and g_y values in all models and additionally displays very minor and non-systematic variations among the large models (see supporting information), so that the present hypothesis cannot be confirmed by a quantitative calculation. Nevertheless, it is interesting to briefly examine the rotations of the

respective Cys-546 and Cys-549 fragments. Rotation of the latter is supported by the ENDOR spectra, rotation of the former would be in-line with the changed g values of Ni-A and Ni-B. These structural rotations of both cysteine fragments are minor. The question as to which structural changes induce a rotation of these fragments by 7-10 degrees may have to be sought further away from the active site. Since Cys-546 is located at the end of the access channel to the active site,⁶⁷ it may well be conceivable that a more remote structural modification of this access channel, e.g., a narrowing or complete closure, induces a small rotation of the Cys-546 residue and strain on the active site while additionally being responsible for the different activation kinetics of the Ni-A and Ni-B states.⁸ The differences in activation rates would then rather result from lowered transportation rates of either H_2 or H^+ in one or both of the channels. This may be particularly the case for the residues that are involved in proton transport. It is unlikely that electron transport is the limiting step of the activation, since the rate limiting step is rather associated with the activation of the Ni-SU state (see scheme 1). Independent of these considerations, the results of this study confirm that small angular changes of the cysteine residues in the [NiFe] center without additional structural modifications suffice to explain the spectroscopic differences between Ni-A and Ni-B in as far as they are observed in EPR, ENDOR and FTIR spectroscopy.

Acknowledgement

The authors thank Dr. Marco Flores and Prof. Frank Neese for helpful discussions during the various stages of this work. This work was financially supported by the Max Planck Society and the EU/Energy Network project SOLAR-H2 (FP7 contract 212508).

References

1. W. B. Tolman, *Activation of Small Molecules: Organometallic and Bioinorganic Perspectives*, Wiley, Weinheim, 2006.
2. W. Lubitz, H. Ogata, O. Rüdiger and E. Reijerse, *Chem. Rev.*, 2014, 114, 4081-4148.
3. P. M. Vignais, B. Billoud and J. Meyer, *FEMS Microbiol. Rev.*, 2001, 25, 455-501.
4. R. Schlögl, *Chemical Energy Storage*, De Gruyter, Berlin, 2013.
5. M. Rögner, *Biohydrogen*, De Gruyter, 2015.
6. D. L. DuBois, *Inorg. Chem.*, 2014, 53, 3935-3960.
7. W. Lubitz, E. Reijerse and M. van Gastel, *Chem. Rev.*, 2007, 107, 4331-4365.
8. V. M. Fernandez, E. C. Hatchikian and R. Cammack, *Biochim. Biophys. Acta*, 1985, 832, 69-79.
9. C. Stadler, A. L. de Lacey, Y. Montet, A. Volbeda, J. C. Fontecilla-Camps, J. C. Conesa and V. M. Fernandez, *Inorg. Chem.*, 2002, 41, 4424-4434.
10. B. Bleijlevens, F. A. van Broekhuizen, A. L. de Lacey, W. Roseboom, V. M. Fernandez and S. P. J. Albracht, *J. Biol. Inorg. Chem.*, 2004, 9, 743-752.
11. T. Krämer, M. Kampa, W. Lubitz, M. van Gastel and F. Neese, *ChemBioChem*, 2013, 14, 1898-1905.
12. M. Stein and W. Lubitz, *J. Inorg. Biochem.*, 2001, 86, 442-442.
13. M.-E. Pandelia, H. Ogata and W. Lubitz, *ChemPhysChem*, 2010, 11, 1127-1140.
14. M. M. van Schooneveld and S. deBeer, *J. Electron. Spectrosc. Relat. Phenom.*, 2015, 198, 31-56.
15. S. Kurkin, S. J. George, R. N. F. Thorneley and S. P. J. Albracht, *Biochemistry*, 2004, 43, 6820-6831.
16. M. van Gastel, M. Stein, M. Brecht, O. Schröder, F. Lenzian, R. Bittl, H. Ogata, Y. Higuchi and W. Lubitz, *J. Biol. Inorg. Chem.*, 2006, 11, 41-51.
17. M. Brecht, M. van Gastel, T. Buhrke, B. Friedrich and W. Lubitz, *J. Am. Chem. Soc.*, 2003, 125, 13075-13083.
18. H. Ogata, S. Hirota, A. Nakahara, H. Komori, N. Shibata, T. Kato, K. Kano and Y. Higuchi, *Structure*, 2005, 13, 1635-1642.
19. R. P. Happe, W. Roseboom, A. J. Pierik, S. P. J. Albracht and K. A. Bagley, *Nature*, 1997, 385, 126-126.
20. A. L. de Lacey, E. C. Hatchikian, A. Volbeda, M. Frey, J. C. Fontecilla-Camps and V. M. Fernandez, *J. Am. Chem. Soc.*, 1997, 119, 7181-7189.
21. A. L. de Lacey, V. M. Fernandez, M. Rousset, C. Cavazza and E. C. Hatchikian, *J. Biol. Inorg. Chem.*, 2003, 8, 129-134.
22. S. J. George, S. Kurkin, R. N. F. Thorneley and S. P. J. Albracht, *Biochemistry*, 2004, 43, 6808-6819.
23. M. van Gastel, M. Stein, M. Brecht, O. Schröder, F. Lenzian, R. Bittl, H. Ogata, Y. Higuchi and W. Lubitz, *J. Biol. Inorg. Chem.*, 2006, 11, 41-51.
24. S. H. Li and M. B. Hall, *Inorg. Chem.*, 2001, 40, 18-24.
25. M. van Gastel, *Appl. Magn. Reson.*, 2010, 37, 207-218.
26. H. Ogata, P. Kellers and W. Lubitz, *J. Mol. Biol.*, 2010, 402, 428-444.
27. A. Pardo, A. L. de Lacey, V. M. Fernandez, Y. Fan and M. B. Hall, *J. Biol. Inorg. Chem.*, 2007, 12, 751-760.

28. A. Volbeda, L. Martin, C. Cavazza, M. Matho, B. W. Faber, W. Roseboom, S. P. J. Albracht, E. Garcin, M. Rousset and J. C. Fontecilla-Camps, *J. Biol. Inorg. Chem.*, 2005, 10, 239-249.
29. P. Amara, A. Volbeda, J. C. Fontecilla-Camps and M. J. Field, *J. Am. Chem. Soc.*, 1999, 121, 4468-4477.
30. M. Pavlov, P. E. M. Siegbahn, M. R. A. Blomberg and R. H. Crabtree, *J. Am. Chem. Soc.*, 1998, 120, 548-555.
31. M. Pavlov, M. R. A. Blomberg and P. E. M. Siegbahn, *Int. J. Quantum Chem.*, 1999, 73, 197-207.
32. L. De Gioia, P. Fantucci, B. Guigliarelli and P. Bertrand, *Int. J. Quantum Chem.*, 1999, 73, 187-195.
33. L. De Gioia, P. Fantucci, B. Guigliarelli and P. Bertrand, *Inorg. Chem.*, 1999, 38, 2658-2662.
34. S. Q. Niu, L. M. Thomson and M. B. Hall, *J. Am. Chem. Soc.*, 1999, 121, 4000-4007.
35. S. Niu and N. B. Hall, *Inorg. Chem.*, 2001, 40, 6201-6203.
36. C. Stadler, A. L. de Lacey, B. Hernandez, V. M. Fernandez and J. C. Conesa, *Inorg. Chem.*, 2002, 41, 4417-4423.
37. M. Stein and W. Lubitz, *Phys. Chem. Chem. Phys.*, 2001, 3, 2668-2675.
38. M. Stein, E. van Lenthe, E. J. Baerends and W. Lubitz, *J. Am. Chem. Soc.*, 2001, 123, 5839-5840.
39. A. Volbeda, L. Martin, E. Barbier, O. Gutierrez-Sanz, A. L. de Lacey, P. P. Liebgott, S. Dementin, M. Rousset and J. Fontecilla-Camps, *J. Biol. Inorg. Chem.*, 2015, 20, 11-22.
40. A. L. de Lacey, V. M. Fernandez, M. Rousset and R. Cammack, *Chem. Rev.*, 2007, 107, 4304-4330.
41. F. Neese, *WIREs Comput. Mol. Sci.*, 2012, 2, 73-78.
42. A. D. Becke, *Phys. Rev. A*, 1988, 38, 3098-3100.
43. J. P. Perdew, *Phys. Rev. B*, 1986, 33, 8822-8824.
44. S. Grimme, J. Antony, S. Ehrlich and H. Krieg, *J. Chem. Phys.*, 2010, 132.
45. S. Grimme, S. Ehrlich and L. Goerigk, *J. Comput. Chem.*, 2011, 32, 1456-1465.
46. C. T. Lee, W. T. Yang and R. G. Parr, *Phys. Rev. B*, 1988, 37, 785-789.
47. R. Izsak and F. Neese, *J. Chem. Phys.*, 2011, 135.
48. E. van Lenthe, J. G. Snijders and E. J. Baerends, *J. Chem. Phys.*, 1996, 105, 6505-6516.
49. E. van Lenthe, A. van der Avoird and P. E. S. Wormer, *J. Chem. Phys.*, 1998, 108, 4783-4796.
50. F. Weigend and R. Ahlrichs, *Phys. Chem. Chem. Phys.*, 2005, 7, 3297-3305.
51. D. A. Pantazis, X.-Y. Chen, C. R. Landis and F. Neese, *J. Chem. Theory Comput.*, 2008, 4, 908-919.
52. A. Klamt and G. Schüürmann, *J. Chem. Soc.-Perkin Trans. 2*, 1993, DOI: 10.1039/p29930000799, 799-805.
53. W. G. Han and L. Noodleman, *Inorg. Chem.*, 2008, 47, 2975-2986.
54. P. E. M. Siegbahn and M. R. A. Blomberg, *Philos. Trans. R. Soc. A-Math. Phys. Eng. Sci.*, 2005, 363, 847-860.
55. C. Fichtner, C. Laurich, E. Bothe and W. Lubitz, *Biochemistry*, 2006, 45, 9706-9716.
56. P. Kellers, M.-E. Pandelia, L. J. Currell, H. Goerner and W. Lubitz, *Phys. Chem. Chem. Phys.*, 2009, 11, 8680-8683.
57. M.-E. Pandelia, H. Ogata, L. J. Currell, M. Flores and W. Lubitz, *Biochim. Biophys. Acta*, 2010, 1797, 304-313.

58. M.-E. Pandelia, H. Ogata, L. J. Currell, M. Flores and W. Lubitz, *J. Biol. Inorg. Chem.*, 2009, 14, 1227-1241.
59. C. Fichtner, M. van Gastel and W. Lubitz, *Phys. Chem. Chem. Phys.*, 2003, 5, 5507-5513.
60. V. Jonas and W. Thiel, *J. Chem. Phys.*, 1995, 102, 8474-8484.
61. V. Jonas and W. Thiel, *Organometallics*, 1998, 17, 353-360.
62. C. Bagyinka, J. P. Whitehead and M. J. Maroney, *J. Am. Chem. Soc.*, 1993, 115, 3576-3585.
63. M. Carepo, D. L. Tierney, C. D. Brondino, T. C. Yang, A. Pamplona, J. Telser, I. Moura, J. J. G. Moura and B. M. Hoffman, *J. Am. Chem. Soc.*, 2002, 124, 281-286.
64. F. Neese, *J. Chem. Phys.*, 2001, 115, 11080-11096.
65. S. Sinnecker and F. Neese, *J. Comput. Chem.*, 2006, 27, 1463-1475.
66. A. J. Stone, *Proc. R. Soc. London, Ser. A*, 1963, 271, 424-434.
67. A. Volbeda and J. C. Fontecilla-Camps, *Coord. Chem. Rev.*, 2005, 249, 1609-1619.